Journal of Power Sources 199 (2012) 22–28

Contents lists available at SciVerse ScienceDirect

Journal of Power Sources

journal homepage: www.elsevier.com/locate/jpowsour

Titanium carbide-derived carbon as a novel support for platinum catalysts in direct methanol fuel cell application

Alicja Schlange[a,*], Antonio Rodolfo dos Santos[a], Benjamin Hasse[b], Bastian J.M. Etzold[b], Ulrich Kunz[a], Thomas Turek[a]

[a] Institute of Chemical Process Engineering, Clausthal University of Technology, Leibnizstr. 17, D-38678 Clausthal-Zellerfeld, Germany
[b] Institute of Chemical Engineering, University of Erlangen-Nuremberg, Egerlandstr. 3, D-91058 Erlangen, Germany

ARTICLE INFO

Article history:
Received 27 June 2011
Received in revised form 22 August 2011
Accepted 29 September 2011
Available online 5 October 2011

Keywords:
Carbide-derived carbon
Novel support material
Catalyst
Direct methanol fuel cell

ABSTRACT

The improvement of direct methanol fuel cells (DMFCs) requires the development of highly active catalysts. Carbide-derived carbon (CDC) is a new class of carbon materials which are produced via selective extraction of the non-carbon compounds from metal carbides. Nanoporous carbon with a surface area of 906 $m^2 g^{-1}$ and mean pore size of 3.4 nm was produced in consequence of chlorinating pure titanium carbide. This material was oxidatively treated to create the nucleation sites for the metal precursor. An increase of oxygen content in the carbon sample was observed after the functionalization step. The CDC material was subsequently loaded with 18.62 wt.% platinum, with an average particle size of 1.16 nm, by wet impregnation and chemical reduction. As a result, an enhanced electrochemical activity towards oxygen reduction was observed. The maximum power density of 50.16 mW cm^{-2} was achieved and is subsequently 18% higher than the value measured for commercial platinum catalyst (20 wt.% Pt) on activated carbon. This increase can be attributed to good catalyst dispersion, high surface area and small platinum cluster sizes, thus, confirming the potential of carbide-derived carbon supported catalysts for DMFC applications.

1. Introduction

Direct methanol fuel cells (DMFCs) have attracted great attention as a promising power source for portable applications due to their high energy density, simple system design and low emissions of pollutants [1–3]. Using liquid methanol as fuel offers many advantages over the hydrogen, such as easier storage and transport at lower costs [4]. However, there are still some factors limiting the widespread commercialization of this kind of fuel cell. The major problems associated with DMFC operation are the slow electrode kinetics of the oxygen reduction reaction and methanol crossover through the polymer membrane.

To improve the fuel cell performance, highly active electrocatalysts have to be developed. It is generally known that catalysts exhibit great influence on the cost and durability of fuel cells. Most catalysts used in DMFCs are supported on porous conductive carbon materials with a high specific surface area. These support materials are necessary to obtain a high dispersion and a narrow distribution of platinum or platinum-alloy nanoparticles, which are essential for a high catalytic performance of fuel cell catalysts [5–9].

Widely, platinum or platinum alloy nanoparticles supported on high surface area carbon blacks are commercially used as DMFC catalysts. Recently, nanostructured carbon materials like carbon nanofibers, carbon nanotubes or mesoporous carbons have been intensively studied as support materials for platinum electrocatalysts in DMFCs [10–13]. The use of novel carbon materials as catalyst support can enhance the mass activity of the catalyst in the cathode oxygen reduction reaction [14].

There are several attributes that carbon materials as supports need to possess to be acceptable for low temperature fuel cell electrocatalysts. These attributes are high surface area for a high degree of dispersion of the nanoparticles, suitable pore structure, good crystallinity resulting in low electrical resistance to facilitate electron transport during the electrochemical reactions, good interaction between the catalyst nanoparticles and the carbon support, high stability in the fuel cell environment and good corrosion resistance [6,15].

In this contribution, we demonstrate the use of carbide-derived carbon (CDC) as an attractive catalyst support material for the electrode of a DMFC. With the carbide-derived carbon method, a new class of carbon materials can be produced from the selective extraction of non-carbon compounds from metal carbides [16–18]. With the CDC method it is possible to convert the carbide partially, with controlled layer thickness, or completely into nanoporous carbon with a defined pore structure and specific surface areas greater than

* Corresponding author. Tel.: +49 5323 722187; fax: +49 5323 722182.
E-mail address: schlange@icvt.tu-clausthal.de (A. Schlange).

0378-7753/$ – see front matter © 2011 Elsevier B.V. All rights reserved.
doi:10.1016/j.jpowsour.2011.09.107

2000 $m^2\ g^{-1}$ [19–21]. Hence, the characteristics of CDC can be tailored towards a specific application. The extraction of the metal can be achieved by using either halogens or supercritical water in a high temperature reaction or vacuum decomposition [22–24]. A promising reaction path is the extraction of the metal species (Me) using chlorine gas:

$$MeC(s) + x/2Cl_2(g) \rightarrow MeCl_x(g) + C(s)$$

In order to selectively extract the metal compounds, the formation of gaseous CCl_4 has to be suppressed either thermodynamically or kinetically. For thermodynamic reasons the reaction temperature has to lie above approximately 400 °C [25–27], as the formation of metal–chloride species then is favoured. Typical reaction temperatures range from 400 to 1200 °C. By choice of the reaction temperature one can influence and tailor the created pore structure. Dash et al. investigated average pore diameter of carbon materials, originating from zirconium carbide, increased with rising reaction temperatures from 0.74 nm at 400 °C to 1.41 nm at 1200 °C [28]. The produced specific surface area is also a function of reaction temperature, featuring a maximum between 800 and 1200 °C for most carbides. This can be explained with halogenide residues clogging pores at low temperatures and CDC consolidation at high temperatures [28,29]. Increased reaction temperature also has an effect on the morphology of the created carbon material. Up to reaction temperatures of approx. 800 °C almost every CDC features amorphous characteristics whereas above 1000 °C more crystalline, graphitic, structures can be generated, depending on the precursor carbide.

In summary, a set of parameters exists with which the characteristics of CDC can be tailored towards its specific application. The choice of the original carbide together with the chlorination temperature determines the created pore and carbon structure. These characteristics make CDC an interesting material in the field of catalyst support for the electrode of direct methanol fuel cell [30].

2. Experimental

2.1. Materials

All chemicals used in this work were analytical grade. As Platinum precursor $H_2PtCl_6{\cdot}6H_2O$ (Merck) was used. HNO_3, polytetrafluoroethylene (Dyneon), ethylene glycol, NaOH and $H_3PMo_{12}O_{40}$ were purchased from Sigma–Aldrich. TiC was purchased from Alfa Aesar with a purity of 99.5% (metal basis).

2.2. Synthesis of titanium carbide-derived carbon support

For this work, TiC–CDC was produced in a tubular reactor at a reaction temperature of 1200 °C. Approx. 6 g of TiC was etched with a chlorine concentration of 2 mol m^{-3} and a gas velocity of 0.015 m s^{-1} inside the reactor. Helium was used to adjust the overall flow rate to 8 NL h^{-1}. The experiment was performed for at least 4 h in order to convert the metal carbide completely to carbon.

2.3. Surface modification of TiC–CDC support

Before Pt deposition, the TiC–CDC material was treated with nitric acid to create oxygen functional groups. In a typical experiment, 5 g of support material was mixed with 150 mL nitric acid (65 wt.%) and refluxed at 110 °C under nitrogen atmosphere for 5 h. The resulting solution was washed with deionized water and centrifuged until the filtrate reached pH 7. Finally, the treated titanium carbide-derived carbon (TiC–CDC_f) material was dried in an oven at 60 °C overnight.

2.4. Preparation of platinum electrocatalyst

The Pt electrocatalyst was prepared using the polyol alcohol reduction method [33,34]. Ethylene glycol (EG) was used as solvent and reducing agent, and $H_3PMo_{12}O_{40}$ was used to prevent Pt particle agglomeration. Typically, $H_2PtCl_6{\cdot}6H_2O$, $H_3PMo_{12}O_{40}$ (weight ratio PMo_{12}:Pt = 1:1) and pretreated carbon support (160 mg) were mixed with 80 mL EG in a beaker and subjected to an ultrasonic bath for 10 min. After that, the pH value of the mixture was adjusted to 10 by adding 1 mol L^{-1} NaOH under vigorous stirring. The amount of Pt precursor was calculated to obtain a nominal metal loading of 40 wt.% after the complete reduction. The suspension was transferred to a 100 mL flask and heated under refluxing conditions at 140 °C for 3 h under continuous magnetic stirring.

After cooling down, the resulting catalyst (Pt/TiC–CDC_f) was washed with ethanol to eliminate traces of chloride ions, which was separated using a centrifuge at 4000 rpm and dried in a furnace at 60 °C for 24 h under air flow.

2.5. Characterization methods

The analysis of the pore volume and pore size distribution was carried out for the CDC after chlorination as well as for the supported catalysts, using CO_2 and N_2 sorption measurements with a Quantachrome Nova 4200e measuring at 273 K, and a Quantachrome QuadrasorbSI measuring at 77 K, respectively. Subsequent data evaluation was performed with the software NovaWin version 10.0 and QuadraWin version 5.02 for CO_2 and N_2 sorptions, using non-local density functional theory (NLDFT) and quenched solid density functional theory (QSDFT) for slit pores, respectively.

The crystalline structures of supported catalysts were characterized by X-ray diffraction (XRD) with a Siemens D5000/Kristalloflex diffractometer in the $\theta/2\theta$ modus using Co-Kα radiation source at λ = 0.1789 nm (40 kV, 40 nA) with particle sizes being determined using the Scherrer equation [31]. The 2θ Bragg angles were scanned over a range from 20° to 80° with a step size of 0.02°.

The morphology and size distribution of the catalyst were carried out using transmission electron microscopy (TEM) with a JEOL 2100 (accelerating voltage 200 kV). TEM samples were prepared by placing a drop of catalyst suspension dispersed in ethanol on a copper grid followed by solvent evaporation at room temperature. Information about size and distribution of the Pt nanoparticles was obtained using LINCE 2.42e software [32] with 300 nanoparticles on the TEM pictures. Thermogravimetric analysis (TGA) was performed with a Mettler TGA 860 thermo balance in air at a flow rate of 50 $cm^3\ min^{-1}$ and a heating rate of 20 K min^{-1} over a temperature range of 25–900 °C using several mg samples. To investigate the oxidized support material, elemental analysis (EA) (Vario-EL, Elementar Analysesyteme GmbH) and scanning electron microscopy (SEM) (Helios Nanolab 600, FEI) investigations were done.

2.6. Electrochemical measurements and electrode preparation

DMFC single cell measurements were evaluated in a test station using a high impedance potentiometer (Delta Elektronika SM3000, The Netherlands). A cell with an active area of 5 cm^2 was used. The catalyst loadings on the cathode and anode side were both 1 mg cm^{-2}. The cathode layer was prepared using a Pt supported TiC–CDC_f catalyst or commercial Pt catalyst (20 wt.% Pt) supported on Vulcan® XC-72R carbon from E-TEK (labeled as Pt/C). In the anode layer a commercial catalyst from BASF (40 wt.% Pt, 20 wt.% Ru on Vulcan® XC-72R carbon) was used.

For the preparation of catalyst coated membrane (CCM), water, catalyst and Nafion® ionomer (15 wt.%) were used at a weight ratio

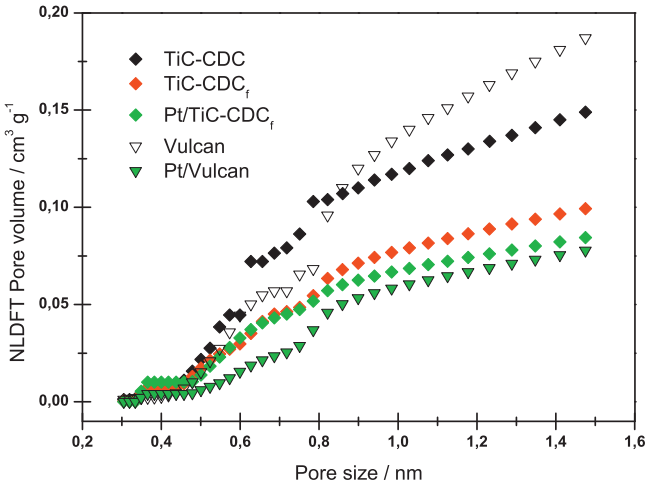

Fig. 1. Non-local density functional theory (NLDFT) pore volume obtained from CO_2 sorption, measured with a Quantachrome Nova 4200e at 273 K. Subsequent data evaluation was performed with the software NovaWin version 10.0 using NLDFT.

of 9:1:1.175. Water was added to the catalyst and submitted to an ultrasonic mixer for 5 min to form a uniform suspension. After that, Nafion® ionomer was added to this suspension and stirred with a magnetic stirrer overnight, resulting in homogeneous distribution of the Nafion® ionomer in the solution. The catalyst ink was sprayed on a Nafion® 117 membrane positioned on a hot plate (120 °C).

Finally, the CCM was hot-pressed at 120 °C with a pressure of 0.14 t cm^{-2} for 3 min. The diffusion layers were fabricated by coating carbon cloth (Ballard, AvCarb 1071HCB) with a layer of 85 wt.% carbon black (Ketjen Black EC 300 J) and 15 wt.% PTFE. Current–voltage measurements were carried out at 80 °C with 5 mL min^{-1} of 1 mol L^{-1} methanol solution being pumped at the anode side while 200 mL min^{-1} of pure oxygen was fed to the cathode side.

3. Results and discussion

3.1. Influence of surface functionalization on the TiC–CDC structure

A treatment of carbon materials with oxidizing agents like HNO_3 may attack the carbon structure and lead to the collapse of specific pore volume and surface area. Since a high surface area is important for enhanced catalytic performance, the influence of the surface modification with HNO_3 on the TiC–CDC structure has to be evaluated. Sorption analysis using CO_2 and N_2 reveal the specific surface area and pore volume thereby indicating pore stability. In order to evaluate the effect of the surface modification, the original support material was analyzed before and after functionalization. To further investigate the changes due to the deposition of platinum on TiC–CDC sorption measurements were conducted after this step as well. The results were compared to sorption analysis of commercially available carbon black and platinum loaded carbon black.

The comparison of CO_2 sorption results, illustrated in Fig. 1, reveals a cumulative micropore volume of 0.187 and 0.149 cm^3 g^{-1} for the commercial carbon black (Vulcan XC-72R) and TiC–CDC respectively. These results indicate a relatively low amount of micropores smaller than 1.5 nm in both materials. For TiC–CDC after 5 h functionalization with boiling nitric acid the micropore volume is reduced to 0.099 cm^3 g^{-1} which can be attributed to partial collapse of pores in the carbon material. For the platinum containing CDC a comparison to the commercial platinum loaded carbon black can be drawn. In this instance the cumulative volume of the commercial catalyst reaches only 0.077 cm^3 g^{-1} compared to 0.084 cm^3 g^{-1} for Pt/TiC–CDC$_f$.

N_2-sorption measurements analyzing pores larger than 1 nm, shown in Fig. 2, indicate similar results. The non-platinum loaded commercial carbon black reaches a specific pore volume of 1.122 cm^3 g^{-1} containing a wide pore size distribution from 2 nm to larger than 20 nm. For the platinum containing carbon black the pore volume is strongly reduced to 0.178 cm^3 g^{-1}. The analysis of the specific surface area also shows a decrease from 738 to 86 m^2 g^{-1} for the platinum loaded one (see Table 1). There is no information about how this commercial material is treated to introduce the metal. Therefore, one cannot say which process is leading to the decrease in specific pore volume and surface area. TiC–CDC reaches a cumulative pore volume of 0.713 cm^3 g^{-1} with pores up to 4 nm and a volume mean pore size of 3.4 nm.

After the functionalization and the deposition of platinum the obtained specific pore volume is reduced to 0.404 and 0.246 cm^3 g^{-1}, respectively. The specific surface area of TiC–CDC declines from originally 906 m^2 g^{-1}–390 m^2 g^{-1} after the functionalization and is even further reduced to 180 m^2 g^{-1} after the deposition of platinum. These results show that during functionalization the originally obtained TiC–CDC pore structure is affected and its specific surface area is drastically reduced. This effect can be explained by the complete oxidation of carbon from pore walls to CO_2 which results in a combination of neighboring pores and thus a lower specific surface area of the CDC after functionalization. The deposition of platinum lowers the accessible pore volume and surface area, which can be explained by clogged pores. These closed pores are not accessible anymore which again reduces the specific surface area of the material and may be a drawback for its application in catalysis. Despite the strong affection of the pore structure during functionalization and clogging of pores within platinum deposition, TiC–CDC still features higher surface area and pore volume compared to the commercial catalyst. These characteristics might lead to lower mass transfer resistance and as a result be advantageous for the application in catalysis.

To investigate macroscopic changes caused by the oxidizing agent HNO_3 on TiC–CDC, SEM pictures were made before and after the functionalization step which are shown in Fig. 3. Picture (a) shows the original CDC and picture (b) shows the carbon material after treatment with nitric acid. Comparing both pictures it seems that surface roughening is caused by the functionalization process. This underlines the statement obtained from the sorption

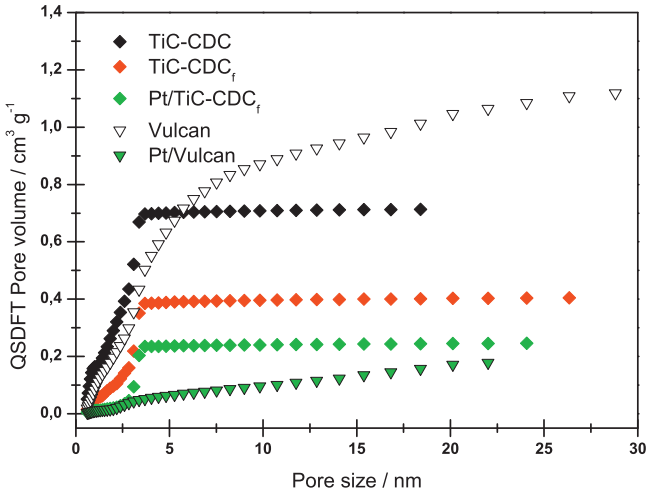

Fig. 2. Quenched solid density functional theory (QSDFT) pore volume obtained from N_2 sorption, measured with a Quantachrome QuadrasorbSI at 77 K. Subsequent data evaluation was performed with the software QuadraWin version 5.02 using QSDFT.

Table 1
QSDFT specific surface area obtained from N_2 sorption analysis.

	TiC–CDC	TiC–CDC_f	Pt/TiC–CDC_f	Vulcan XC-72R	Pt/C
QSDFT specific surface area ($m^2\ g^{-1}$)	906	390	180	738	86

experiments that the functionalization conditions used in this work lead to a decomposition of the carbon structure which reduces the specific surface area. Less harsh functionalization conditions may improve the preservation of the original TiC–CDC structure and have to be studied in future work as well as investigations concerning mass transfer resistance during catalysis.

3.2. Elemental analysis and TGA for CDC

The functionalization step for CDC is necessary, following the chlorination of the surface, the received material shows few functional groups, probably chemisorbed chlorine [35]. By chemical oxidation with nitric acid functional groups are introduced on the carbon surface, which promote nucleation sites for Pt nanoparticles reduction. These oxygen-containing groups are mainly carboxyl (COOH), hydroxyl (O–H) and carbonyl (C=O) groups [35–39].

The increase in surface oxygen for TiC–CDC by the oxidative treatment with nitric acid was examined by elemental analysis (EA), the results are given in Table 2. They indicate that the oxygen concentration increases after oxidative treatment from 2.36% to 16.98% while the carbon content in the sample decreases from 97.34% to 81.42%, which can be explained by the formation of functional groups on the TiC–CDC surface.

Table 2
Results of elemental analysis for TiC–CDC and TiC–CDC_f samples.

	C (wt.%)	H (wt.%)	N (wt.%)	O (wt.%)	C/O
TiC–CDC	97.34	0.25	0.04	2.36	41.15
TiC–CDC_f	81.42	1.43	0.16	16.98	4.79

Thermogravimetric analysis (TGA) was used to investigate the thermal stability of the samples. It can be seen that the untreated TiC–CDC is thermally stable in air up to a temperature of 580 °C (see Fig. 4), at higher temperatures the carbon material is burned off. In contrast, the functionalized material TiC–CDC_f starts to decompose at lower temperature due to the presence of oxygen containing groups. In the temperature range between 150 °C and 350 °C a weight loss of 5.14% is observed, which can be attributed to the decarboxylation of carboxylic acid groups [40]. The thermal degradation in the range between 350 °C and 500 °C can be attributed to the elimination of hydroxyl groups from the carbon surface [40].

The platinum loaded sample starts to decompose at a lower temperature since platinum is a catalyst for carbon oxidation. For the platinum loaded carbon (Pt/TiC–CDC_f) a residue of 18.75 wt.% corresponds to the platinum content in the sample. This result was confirmed via the quantitative analysis by ICP, where 18.62 wt.% Pt was found. Hence, the yield of noble metal from the precursor solution is approx. 47% after all steps. To achieve a higher Pt loading on the support material a modification of the polyol method is needed. One idea to improve the dispersion of the platinum particles is the application of ultrasound. The other aspect of interest is the adjustment of the pH value as there is information in the literature that this parameter also influences platinum loading [41]. It has to be studied in future work.

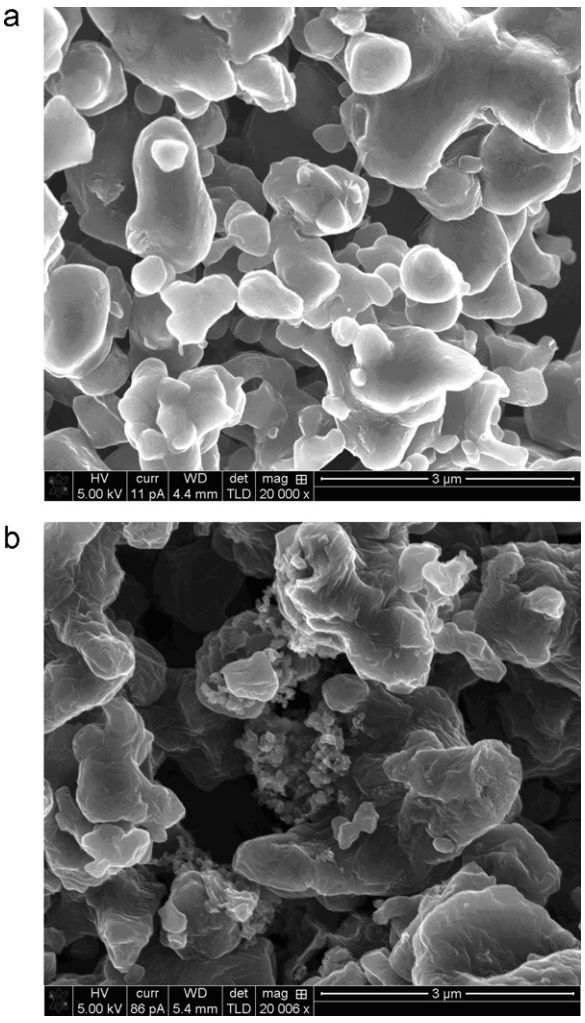

Fig. 3. Comparison of TiC–CDC before (a) and after functionalization (b) using 5 g of support, 150 mL nitric acid (65%), refluxed at 110 °C in nitrogen atmosphere for 5 h.

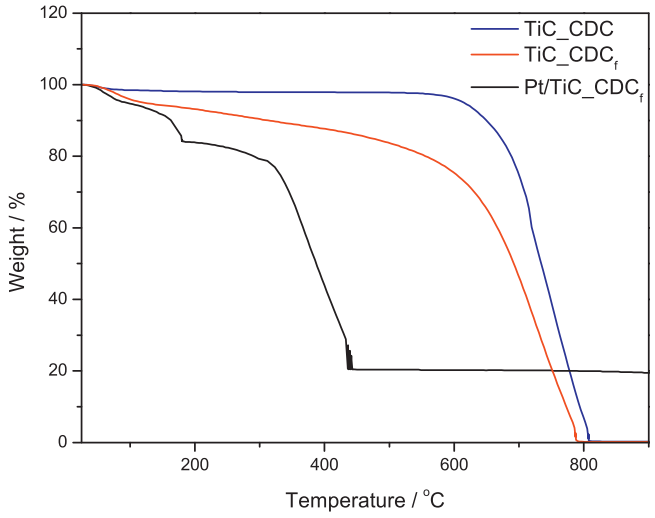

Fig. 4. TGA profiles of TiC–CDC, TiC–CDC_f and Pt/TiC–CDC_f samples.

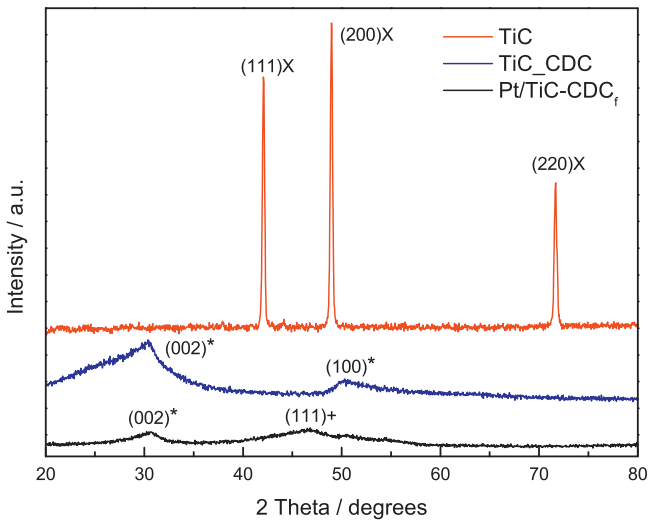

Fig. 5. X-ray diffraction patterns for TiC, TiC–CDC and Pt/TiC–CDC_f powders, ×TiC, *graphitic structures and +platinum.

3.3. XRD patterns

Powder X-ray diffraction (XRD) analysis was done to investigate the structural changes in the sample after the chlorination process, the diffraction patterns are shown in Fig. 5. For TiC, characteristic diffraction peaks at 42.0°, 48.9° and 71.6° were observed, which correspond to (1 1 1), (2 0 0) and (2 2 0) reflections of the TiC fcc structure, respectively [42–44]. For TiC–CDC, characteristic diffraction peaks at 30.4° and 50.4° can be attributed to (0 0 2) and (1 0 0) reflections of the graphite plane. After chlorination no presence of TiC residue or crystalline graphite was observed, revealing the complete transformation of TiC to nanoporous carbon powder. The absence of TiC in the nanoporous carbon sample was additionally confirmed by EDX analysis.

For the Pt/TiC–CDC_f sample, two characteristic peaks at 30.4° and 46.6° were found, which correspond to (0 0 2) graphite and (1 1 1) platinum planes, respectively. The XRD measurements were done with a diffractometer using Co-Kα as the radiation source. For this reason the Pt (1 1 1) peak is occurring at higher position than by using Cu-Kα.

Despite the high chlorination temperature of 1200 °C the TiC–CDC features broad peaks corresponding to (0 0 2) and (1 0 0) graphite planes indicating a relatively low degree of crystallinity [44–47]. The graphite crystallite size L_c was calculated from the peak broadening (FWHM) of the (0 0 2) peak with a Scherrer factor of 0.91 and L_a from the (1 0 0) peak and a factor of 1.84, to 2.9 and 5.68 nm, respectively [48].

Hence, TiC–CDC synthesized at 1200 °C shows an amorphous sp2 structure with some degree of graphitic low range ordering, as reported in literature. This graphitic structure can affect the electrochemical performance e.g. due to lower resistance. The Pt/TiC–CDC_f sample contains Pt particles smaller than 2 nm in size resulting in broad peaks. A particle size evaluation using Scherrer equation and a Scherrer factor of 0.91 leads to a mean particle size of 1.09 nm. Additionally particle size evaluation here was performed using TEM pictures. For commercial Pt/C catalyst (not shown in Fig. 5) the Pt particle size calculated with the Scherrer equation was 3.21 nm.

3.4. TEM analysis

In Fig. 6 TEM micrographs of catalyst samples are depicted including particle size histograms and the average particle size.

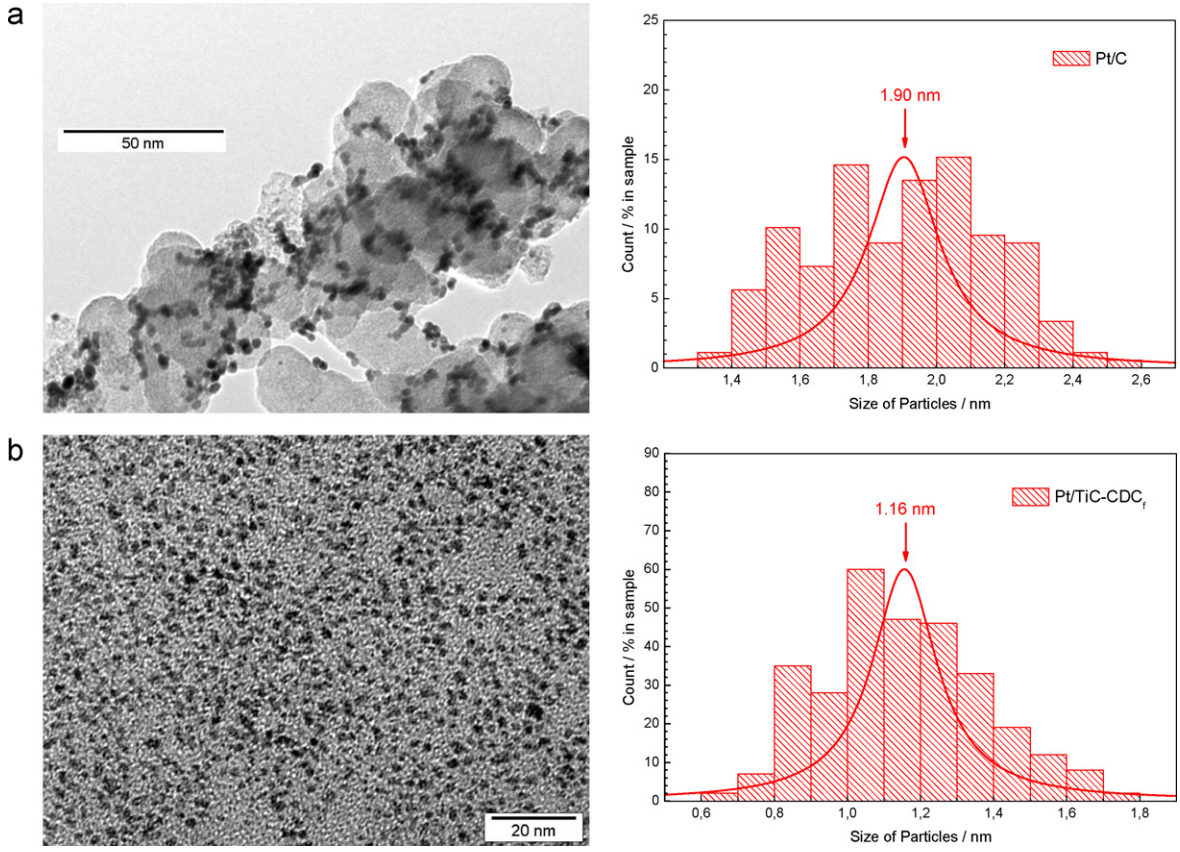

Fig. 6. TEM micrographs of catalyst samples: (a) Pt/C and (b) Pt/TiC–CDC_f catalyst.

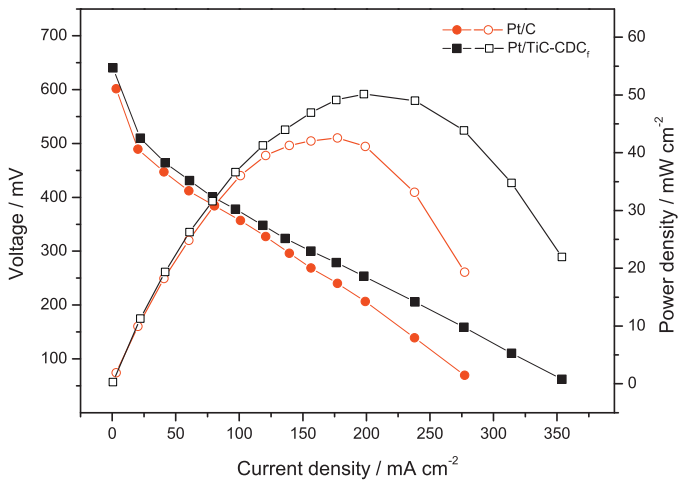

Fig. 7. Comparison of performance in DMFC using Pt/C and Pt/TiC–CDC$_f$ cathode catalyst. Cell with 5 cm^2 at 80 °C, operating with 5 mL min^{-1} of 1 mol L^{-1} methanol and 200 mL min^{-1} of pure oxygen. CCM's manufactured with the same commercial anode catalyst (PtRu/C BASF, 40 wt.% Pt, 20 wt.% Ru) on Nafion® 117 membrane.

For the carbon black supported catalyst a mean platinum particle size of 1.90 nm was estimated. Some areas of the support materials are not covered with metal particles indicating an inhomogeneous distribution of particles. The Pt/TiC–CDC$_f$ catalyst showed a very homogeneous and uniform particle size distribution with a mean particle size of 1.16 nm. Smaller catalyst particles should lead to an increased catalytic activity at equally introduced amounts of platinum, which has to be investigated in DMFC test runs.

3.5. DMFC measurements

The performance of a single DMFC using commercial carbon black and carbide-derived carbon as support materials for oxygen reduction catalysts are shown in Fig. 7. The measurements for both catalysts were done under the same operating conditions. The real platinum loading for both cathode and anode was 1 mg cm^{-2}. The measured open circuit voltage (OCV) of the DMFC with Pt/TiC–CDC$_f$ was with 640.4 mV higher than the observed 601.9 mV for Pt/C standard catalyst, despite the platinum loading for the Pt/TiC–CDC$_f$ reaching only 18.62%. The current densities at 400.0 mV were found to be 78.9 mA cm^{-2} for Pt/TiC–CDC$_f$ and 68.6 mA cm^{-2} for Pt/C, respectively.

It is also shown in Fig. 7 that the cell with the standard catalyst exhibited a maximum power density of 42.58 mW cm^{-2}. If this value is compared to the value of 50.16 mW cm^{-2} obtained for the cell using the new catalyst Pt/TiC–CDC$_f$, an increase of performance of 18% could be achieved using CDC as catalyst support. This improved performance can be related to the good catalysts dispersion, a higher surface area of TiC–CDC$_f$ support, the smaller platinum particles sizes compared to carbon black supported catalyst and the more graphitic ordering of TiC–CDC reducing the electric resistance.

4. Conclusion

Titanium carbide-derived carbon (TiC–CDC) was successfully used as an electrocatalyst support material for DMFC application. Before metal deposition, the surface functionalization of this porous carbon was carried out. The oxidative treatment with nitric acid of TiC–CDC increased the oxygen concentration, in parallel the carbon content in the sample was decreasing, promoting a formation of functional groups on the TiC–CDC surface. Additionally the specific pore volume and surface area were reduced during functionalization but were still slightly higher compared to the commercially available platinum containing carbon black.

The carbon support material obtained after chlorination and functionalization process allowed to prepare a Pt/TiC–CDC$_f$ catalyst with a mean Pt particle size of 1.16 nm. The results of TGA, XRD and TEM revealed a successful deposition of platinum on CDC. The Pt/TiC–CDC$_f$ catalyst showed a very homogeneous and uniform particle sizes distribution with a smaller particle size compared to commercial carbon black. The maximum area related power density of a direct methanol fuel cell using carbide-derived carbon as support material for oxygen reduction increased by 18% in comparison to a commercial catalyst supported on carbon black.

The study showed that TiC–CDC supported noble metal catalysts show better performance during fuel cell application than a commercial catalyst, even without optimization of the catalyst and support. This improved performance, already indicates that carbide-derived carbon is a very promising material as support in direct methanol fuel cell applications. Nevertheless, future experiments will focus on the production of TiC–CDC containing even higher amounts of platinum at larger specific surface areas than achieved in this work and to find the optimum characteristics for CDC in DMFC application. In order to confirm the stability of these catalysts long time experiments in direct methanol fuel cells are necessary.

Acknowledgements

The authors thank the Energy Research Centre of Lower Saxony (Energie-Forschungszentrum Niedersachsen) for financial support of part of this work. The authors also thank the Institute of Nonmetallic Materials at Clausthal University of Technology for SEM investigations and the Institute of Technical Chemistry at Clausthal University of Technology for EA and TGA measurements.

Bastian Etzold and Benjamin Hasse gratefully acknowledge the funding of the German Research Council (DFG), which, within the framework of its 'Excellence Initiative', supports the Cluster of Excellence 'Engineering of Advanced Materials' (www.eam.uni-erlangen.de) at the University of Erlangen-Nuremberg.

References

[1] A.S. Aricò, S. Srinivasan, V. Antonucci, Fuel Cells 1 (2001) 133–161.
[2] S.C. Thomas, X. Ren, S. Gottesfeld, P. Zelenay, Electrochim. Acta 47 (2002) 3471–3478.
[3] H. Chang, S.H. Joo, C. Pak, J. Mater. Chem. 17 (2007) 3078–3088.
[4] B.D. McNicol, D.A.J. Rand, K.R. Williams, J. Power Sources 83 (1999) 15–31.
[5] J.M. Liu, S.J. Liao, Fuel Cells 5 (2007) 402–407.
[6] E. Antolini, Appl. Catal. B: Environ. 88 (2009) 1–24.
[7] J.S. Yu, S. Kang, S.B. Yoon, G.S. Chai, J. Am. Chem. Soc. 124 (2002) 9382–9383.
[8] H. Liu, C. Song, L. Zhang, J. Zhang, H. Wang, D.P. Wilkinson, J. Power Sources 155 (2006) 95–110.
[9] K.I. Han, J.S. Lee, S.O. Park, S.W. Lee, Y.W. Park, H. Kim, Electrochim. Acta 50 (2004) 791–794.
[10] G. Wu, L. Li, J.H. Li, B.Q. Xu, J. Power Sources 155 (2006) 118–127.
[11] J.F. Lin, V. Kamavaram, A.M. Kannan, J. Power Sources 195 (2010) 466–470.
[12] M. Sakthivel, A. Schlange, U. Kunz, T. Turek, J. Power Sources 195 (2010) 7083–7089.
[13] P.V. Shanahan, L. Xu, C. Liang, M. Waje, S. Dai, Y.S. Yan, J. Power Sources 185 (2008) 423–429.
[14] W. Li, C. Liang, W. Zhou, J. Qiu, H. Li, G. Sun, Q. Xin, Carbon 42 (2004) 423–460.
[15] W. Li, C. Li, W. Zhou, J. Qiu, Z. Zhou, G. Sun, Q. Xin, J. Phys. Chem. B 107 (2003) 6292–6299.
[16] Y. Gogotsi, I.D. Jeon, M.J. McNallan, J. Mater. Chem. 7 (1997) 1841–1848.
[17] Y. Gogotsi, A. Nikitin, H. Ye, W. Zhou, J.E. Fischer, B. Yi, H.C. Foley, M.W. Barsoum, Nat. Mater. 2 (2003) 591–594.
[18] F. Glenk, T. Knorr, M. Schirmer, S. Gütlein, B.J.M. Etzold, Chem. Eng. Technol. 33 (2010) 698–703.
[19] V. Presser, M. Heon, Y. Gogotsi, Adv. Funct. Mater. 21 (2011) 810–833.
[20] S.H. Yeon, P. Reddington, Y. Gogotsi, J.E. Fischer, C. Vakifahmetoglu, P. Colombo, Carbon 48 (2010) 201–210.
[21] M. Schmirler, F. Glenk, B.J.M. Etzold, Carbon 49 (2011) 3679–3686.
[22] A. Jänes, T. Thomberg, H. Kurig, E. Lust, Carbon 47 (2009) 23–29.
[23] M. Kormann, H. Gerhard, N. Popovska, Carbon 47 (2009) 242–250.

[24] P. Becker, F. Glenk, M. Kormann, N. Popovska, B.J.M. Etzold, Chem. Eng. J. 159 (2010) 236–241.
[25] S.H. Yeon, S. Osswald, Y. Gogotsi, J.P. Singer, J.M. Simmons, J.E. Fischer, M.Á. Lillo-Ródenas, A. Linares-Solano, J. Power Sources 191 (2009) 560–567.
[26] M. Kormann, H. Ghanem, H. Gerhard, N. Popovska, J. Eur. Ceram. Soc. 28 (2008) 1297–1303.
[27] Y. Gogotsi, Nanomaterials Handbook, Taylor & Francis, Boca Raton, 2006, p. 239–282.
[28] R.K. Dash, G. Yushin, Y. Gogotsi, Micropor. Mesopor. Mater. 86 (2005) 50–57.
[29] R.K. Dash, A. Nikitin, Y. Gogotsi, Micropor. Mesopor. Mater. 72 (2004) 203–208.
[30] Patent WO 2009/045879 A2, published 09.04.2009, Electrocatalysts For Fuel Cells, Applicant: Drexel University, Philadelphia, US, Inventors: Y.A. Elabd, Y. Gogotsi, B. Eirich, D. Shay.
[31] P. Scherrer, Nachrichten von der Königlichen Gesellschaft der Wissenschaften zu Göttingen, vol. 26, 1918, p. 98–100.
[32] S.L.D. Lucato, LINCE 2.4.2e, Department of Materials Science, Darmstadt University of Technology, 1998.
[33] E.V. Spinacé, A. Oliveira-Neto, T.R.R. Vasconcelos, M. Linardi, J. Power Sources 137 (2004) 17–23.
[34] E.V. Spinacé, A. Oliveira-Neto, M. Linardi, J. Power Sources 124 (2003) 426–431.
[35] C. Portet, D. Kazachkin, S. Osswald, Y. Gogotsi, E. Bourguet, Thermochim. Acta 497 (2010) 137–142.
[36] J.L. Figueiredo, M.F.R. Pereira, M.M.A. Freitas, J.J.M. Orfao, Carbon 37 (1999) 1379–1389.
[37] A.E. Aksoylu, M. Madalena, A. Freitas, M.F.R. Pereira, J.L. Figueiredo, Carbon 39 (2001) 175–185.
[38] Y. Otake, R.G. Jenkins, Carbon 31 (1993) 109–121.
[39] M. Sato, M. Ohta, M. Sakaguchi, Electrochim. Acta 35 (1990) 945–950.
[40] V. Datsyuk, M. Kalyva, K. Papagelis, J. Parthenios, D. Tasis, A. Siokou, I. Kallitsis, C. Galiotis, Carbon 46 (2008) 833–840.
[41] H.-S. Oh, J.-G. Oh, H. Kim, J. Power Sources 183 (2008) 600–603.
[42] P. Baveria, S. Harel, H. Garem, M. Grosbras, Scr. Mater. 44 (2001) 2721–2727.
[43] H.T. Bae, J.H. Jeong, H.J. Choi, D.S. Lim, J. Ceram. Soc. Jpn. 118 (2010) 1150–1153.
[44] R. Dash, J. Chmiola, G. Yushin, Y. Gogotsi, G. Laudisio, J. Singer, J. Fischer, S. Kucheyev, Carbon 44 (2006) 2489–2497.
[45] A.R. dos Santos, M. Carmo, A. Oliveira-Neto, E.V. Spinacé, J.G.R. Poço, C. Roth, H. Fuess, M. Linardi, Ionics 14 (2008) 43–51.
[46] M. Carmo, A.R. dos Santos, J.G.R. Poço, M. Linardi, J. Power Sources 173 (2007) 860–866.
[47] S.H. Yeon, I. Knoke, Y. Gogotsi, J.E. Fischer, Micropor. Mesopor. Mater. 131 (2010) 423–428.
[48] B.E. Warren, P. Bodenstein, Acta Crystallogr. 18 (1965) 282–286.